THE DESIGN OF A SINGLE DEGREE OF FREEDOM OPEN-LOOP SPATIAL MECHANISM THAT INCORPORATES GEARED CONNECTIONS

By

JOSEPH M. BARI

A THESIS PRESENTED TO THE GRADUATE SCHOOL
OF THE UNIVERSITY OF FLORIDA IN PARTIAL FULFILLMENT
OF THE REQUIREMENTS FOR THE DEGREE OF
MASTER OF SCIENCE

UNIVERSITY OF FLORIDA

2009

To my mom, for inspiring me to investigate the world, and to my dad, for providing me the foundation to do so

ACKNOWLEDGEMENTS

I would like to acknowledge the support of my committee Dr. Scott Banks, Dr. Carl Crane, Dr. David Dooner and Dr. John Schueller. Dr. Dooner provided invaluable day-to-day support as well as the wonderful Ingear software that made this work possible. Dr. Crane has provided a vast amount of insight and dedication to this project.

I would also like to thank the members of the Center for Intelligent Machines and Robotics for their friendship and knowledge. Finally, I would like to thank my family for their support and love as well as the foundation that has enabled me to reach this point. Thank you to my mom, Gayle Bari, brothers Shane Bari and Adam Reinardy, sister Kaela Reinardy and my amazing girlfriend Carly Knoell.

TABLE OF CONTENTS

page

LIST OF TABLES

LIST OF FIGURES

Abstract of Thesis Presented to the Graduate School
of the University of Florida in Partial Fulfillment of the
Requirements for the Degree of Master of Science

THE DESIGN OF A SINGLE DEGREE OF FREEDOM OPEN-LOOP SPATIAL MECHANISM THAT INCORPORATES GEARED CONNECTIONS

By

Joseph M. Bari

December 2009

Chair: Carl D. Crane, III
Major: Mechanical Engineering

A means has been discovered to apply gear pairing to create a one degree of freedom open-loop spatial mechanism. A specially chosen geometry consisting of three pairs of parallel joint axes is constricted by five sets of gears, three of which are planar, allowing for a reconfigurable mechanism that is suited for repetitive tasks. Previous work has examined three-dimensional rigid body guidance in closed-loop geared mechanisms, but has not come to a solution for the open-loop case.

Two design methods are introduced for the synthesis of mechanism parameters. Gear pairs are designed based upon a desired position and orientation path. Numerical optimization is performed to obtain physically realizable gear profiles. Non-circular gear centrodes must be continuous and smooth. A gear pair must spin in a single direction and with consistent relative turning direction between joined gears. These constraints eliminate non-realizable or non-optimal gears in favor of simple, more easily produced profiles. In the first design algorithm variable parameters include link lengths, joint offsets and twist angles.

A second algorithm is developed that also determines the mechanism parameters and gear profiles that move the end effector through specified positions and orientations

without concern for the path that is followed between poses. Again, gear centrodes must be continuous, smooth and mono-directional. Path freedom allows greater flexibility in the design space of the mechanism. Similar to the rigid path design algorithm, variable parameters are mechanism link lengths, joint offsets and twist angles. The position and orientation of the base of the manipulator are also considered as variable parameters.

CHAPTER 1
INTRODUCTION

1.1 Motivation

Robotic manipulators are utilized for a wide variety of tasks including surgical assistance, weapons disposal and hazardous waste removal. The most common use for manipulators is in an industrial setting. In this setting, motion is often repetitious. Currently, industrial robots achieve this repetitive motion with a series of controllers consisting of electronics and actuators. These systems require overhead in resources and engineering time.

The development of a single degree of freedom manipulator would allow the electronics and actuators to be replaced by mechanical gearing. This would reduce the cost and increase repeated precision as the mechanism is not subject to electronic glitches or pneumatic failure.

A novel mechanism has been developed that allows gear pairs to mechanically couple the variable joint angles in an open-loop manipulator comprised of six revolute joints(6R) and six serial links. The general 6R manipulator has six degrees of freedom; this is constricted to a single degree of freedom by the gears.

Non-circular gearing is utilized to achieve predefined position and orientation requirements of the manipulator's end effector. For physical realization purposes, gear centrodes must be continuous and smooth. In addition, gear pairs must move in a single relative direction. These constraints lead to the design of a mechanism that is capable of moving through a series of ordered desired positions and orientations.

1.2 Related Work

Non-circular gearing has been studied notably by Dooner and Seireg (1995) , who developed a unified geometric theory for the design and manufacturing of gears. The method described is useful for a variety of gearing needs including general non-circular gears. Danieli and Mundo (2004) also developed a method for the design of non-circular gears with constant pressure angle teeth.

Manipulators with mechanically bound joints have been studied previously in both open-loop planar and closed-loop cases. Pang and Krovi (2000) studied both design and number synthesis. They attempted to achieve a desired tool path by the design of mechanism link lengths. However, they did not constrain the number of serial links. They used Fourier techniques to determine the optimal amount of links needed to trace a specified path. The mechanism is limited to movement on a single plane. Krovi, et al. (2002) developed an open-loop planar single degree of freedom serial chain that was coupled using both gear-trains and belt drives. Their mechanism consisted of three revolute joints with parallel joint axes. This allowed coupling between all three joints, but limited the workable area of the manipulator to a single plane perpendicular to the joint axes. Rodriguez et al. (2006) investigated the use of a bound open-loop serial mechanism to create a single degree of freedom anthropomorphic finger. The mechanism consists of three revolute joints bound with tendons similar to those found in a human hand. The tendon-coupling of joints allowed for accurate and human-like grasping by a set of mechanical fingers.

Molder, et al. (2009b) investigated non-circular gears for coupling joints in a five degree of freedom closed-loop manipulator with broad applications. Dooner (2001) studied the use of non-circular gears in the design of gear trains with a specific torque

curve or highly nonlinear Input-Output relationship. Mckinley, et al. (2007) used screw theory techniques to solve the reverse kinematic analysis for the special case 6R mechanism with three sets of parallel joint axes using the unified method defined by Duffy and Rooney (1975). The solution leads to sixteen separate solution sets for a given desired position and orientation. Mckinley (2008) worked further on designing non-circular gears for a closed-loop serial manipulator made up of two sets of the special 6R geometry. Harshe (2009) advanced the design of the closed-loop mechanism with the development of a scoring function for design synthesis optimization. Dou and Ting (1996) defined criterion for serial chain design that is robust against the branching errors inherent to a mechanism with a higher order of reverse analysis solutions.

CHAPTER 2
PROBLEM STATEMENT

Given an ordered set of desired positions and orientations, a mechanism is to be designed that is capable of achieving each successive pose in order. Variable mechanism parameters include three joint offsets, three link lengths and two twist angles. All other offsets, link lengths and twist angles are zero by virtue of the special 6R geometry. The special geometry is pictured in Figure 2-1, and design parameters are displayed in Table 2-1. Joint offset vectors $\boldsymbol{S_1}$ and $\boldsymbol{S_2}$ are parallel, as are $\boldsymbol{S_3}$ and $\boldsymbol{S_4}$ and $\boldsymbol{S_5}$ and $\boldsymbol{S_6}$.

Interior and exterior concentric cylindrical links are utilized, allowing interior links to spin freely inside of exterior links. The exterior links are rigidly attached to the non-planar gears while the interior links are rigidly attached to the planar gear pairs.

Five pairs of non-circular gears are utilized to couple adjacent joints. This reduces the mobility of the mechanism to one, producing a mechanism with a single input necessitating external actuation. In order to design a mechanism with gears that are physically realizable, gear profiles are optimized to be as close to circular as possible. Also, gears must be without abrupt jumps or direction changes. Gears in mesh must move in a single direction, and the input gear motion must also be mono-directional.

Table 2-1. Design parameters

Offset distance (cm)	Link lengths (cm)	Twist angles (degrees)
S_2	a_{12}	$\alpha_{12} = 0$
$S_3 = 0$	$a_{23} = 0$	α_{23}
S_4	a_{34}	$\alpha_{34} = 0$
$S_5 = 0$	$a_{45} = 0$	α_{45}
S_6	a_{56}	$\alpha_{56} = 0$

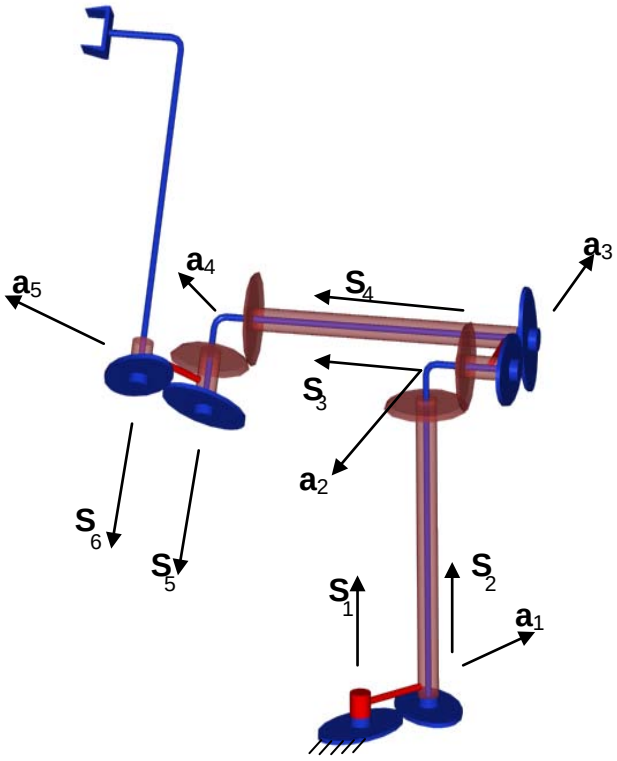

Figure 2-1. Example of open-loop geared manipulator

CHAPTER 3
OPTIMIZATION

Dimensional optimization is performed to minimize a scoring function. The precise scoring function used in this research is discussed in Chapter 4. Nine parameters are optimized including three link lengths (a_{12}, a_{34}, a_{56}), three joint offsets (S_2, S_4, S_6), and two twist angles $(\alpha_{23}, \alpha_{34})$. The reverse kinematic analysis produces sixteen possible solutions, or branches. The branch number is also chosen as a parameter as a different branch may provide drastically different circularity scores.

First, a genetic algorithm optimization is performed with the use of the Matlab “ga” function. A genetic algorithm is chosen to avoid the many local minima present in the highly nonlinear scoring function. The algorithm creates a binary string representative of a vector of parameters and creates an initial random population of parameter values within a specified range. Next, bits in the binary parametric representations of the initial population are swapped with other parameter sets to create the next “generation” of solutions. This process is iterated over successive generations, with solutions with lower scores having a higher probability of surviving to the next generation. Periodically, a random mutation is performed by switching bit values of a solution.

The initial population of the genetic algorithm is designated with a high level of diversity in order to cover the entire design space. This plays a large role in the success of the genetic algorithm.

Because the genetic algorithm is seeded by a random initial population, solutions are not consistent. For this reason, the optimization is run multiple times and the best solution selected. There is no guarantee that the score returned by the genetic algorithm is the absolute minimum, only a high probability that the solution set is close

to the optimal solution. For this reason, an active-set quasi-Newton minimizing optimization is performed with the initial value returned by the genetic algorithm.

The minimizing optimization is performed with the Matlab “fmincon” function. The approximate Hessian matrix is computed, and the search follows the path that alters the parametric vector in order to decrease the scoring function the most. The Hessian matrix is composed of the approximated gradient field of the scoring function with respect to the parametric set and is defined in Equation 3-1.

$$\boldsymbol{H}(f) = \begin{bmatrix} \frac{\partial^2 f}{\partial x_1^2} & \frac{\partial^2 f}{\partial x_1 \partial x_2} & \cdots & \frac{\partial^2 f}{\partial x_1 \partial x_9} \\ \frac{\partial^2 f}{\partial x_2 \partial x_1} & \frac{\partial^2 f}{\partial x_2^2} & \cdots & \frac{\partial^2 f}{\partial x_2 \partial x_9} \\ \vdots & \vdots & \ddots & \vdots \\ \frac{\partial^2 f}{\partial x_9 \partial x_1} & \frac{\partial^2 f}{\partial x_9 \partial x_2} & \cdots & \frac{\partial^2 f}{\partial x_9^2} \end{bmatrix} \qquad (3-1)$$

The quasi-Newton algorithm finds the minimum value of the scoring function within close proximity to the parametric solution returned by the genetic algorithm.

CHAPTER 4
EXACT PATH SPECIFICATION

4.1 Path Creation

A desired path is defined by a series of ordered precision poses, that is, the exact position and orientation requirements for the end effector. These poses are described by a position vector ${}^{F}P_{tool}$, the position of the tool point in the fixed coordinate system and a 3×3 rotation matrix describing the relative orientation of the coordinate system attached to the sixth link and the fixed coordinate system, ${}^{F}_{6}R$. The matrix ${}^{F}_{6}R$ is defined in Equation 4-1.

$$ {}^{F}_{6}\boldsymbol{R} = [\ {}^{F}\boldsymbol{a}_{67}\ {}^{F}\boldsymbol{S}_{6} \times {}^{F}\boldsymbol{a}_{67}\ {}^{F}\boldsymbol{S}_{6}\ ] \qquad (4-1) $$

The rotation matrix and location vector are combined into a 4×4 transformation matrix described by Crane and Duffy (1998) as Equation 4-2.

$$ {}^{F}_{6}\boldsymbol{T} = \begin{bmatrix} {}^{F}_{6}\boldsymbol{R} & {}^{F}\boldsymbol{P}_{6orig} \\ 0\ \ 0\ \ 0 & 1 \end{bmatrix} \qquad (4-2) $$

where:

$$ {}^{F}\boldsymbol{P}_{6orig} = {}^{F}\boldsymbol{P}_{tool} - ({}^{6}\boldsymbol{P}_{tool} \cdot \hat{\boldsymbol{\imath}})^{F} - ({}^{6}\boldsymbol{P}_{tool} \cdot \hat{\boldsymbol{\jmath}})^{F}\boldsymbol{S}_{6} \times {}^{F}\boldsymbol{a}_{67} - ({}^{6}\boldsymbol{P}_{tool} \cdot \hat{\boldsymbol{k}})^{F}\boldsymbol{S}_{6} \qquad (4-3) $$

The desired Cartesian coordinates of the origin of the coordinate system attached to the sixth link are easily obtained from the fourth column of the transformation matrix. Roll (α), pitch (β) and yaw (γ) angles are derived by Crane and Duffy as Equation 4-4.

$$ {}^{F}_{6}\boldsymbol{R} = \begin{bmatrix} r_{11} & r_{12} & r_{13} \\ r_{21} & r_{22} & r_{23} \\ r_{31} & r_{32} & r_{33} \end{bmatrix} \qquad (4-4) $$

where:

$r_{11} = \cos(\beta)\cos(\gamma)$

$r_{12} = -\cos(\beta)\sin(\gamma)$

$r_{13} = \sin(\beta)$

$r_{21} = \cos(\alpha)\sin(\gamma) + \sin(\alpha)\sin(\beta)\cos(\gamma)$

$r_{22} = \cos(\alpha)\cos(\gamma) + \sin(\alpha)\sin(\beta)\cos(\gamma)$

$r_{23} = -\cos(\beta)\sin(\alpha)$

$r_{31} = \sin(\alpha)\sin(\gamma) - \cos(\alpha)\sin(\beta)\cos(\gamma)$

$r_{32} = \sin(\alpha)\sin(\gamma) - \cos(\alpha)\sin(\beta)\cos(\gamma)$

$r_{33} = \cos(\beta)\cos(\alpha)$

${}^{F}_{6}R$ is full rank, so values for α, β, γ can be found from Equation 4-5.

$$\beta = \operatorname{asin}(r_{11})$$

$$\alpha = \operatorname{atan}\left(\frac{\frac{-r_{23}}{cos(\beta)}}{\frac{r_{33}}{cos(\beta)}}\right) \qquad (4-5)$$

$$\gamma = \operatorname{atan}\left(\frac{\frac{-r_{12}}{\cos(\beta)}}{\frac{r_{11}}{\cos(\beta)}}\right).$$

The relative distance between precision points is calculated as a combination of translational and angular displacement. To compensate for unitary disagreement, a scalar mapping metric is chosen to compare the relative change in angular displacement with the relative change in Cartesian displacement. The path is parameterized with a variable t such that when $t = 0$ roll, pitch and yaw angles calculated in Equation 4-5 are with respect to the first pose and when $t = 1$ rotation

angles are calculated with respect to the final pose. The mapping metric affects what value t will have at each of the intermediate poses.

A continuous path is then created by creating splines between precision points. These splines are numerically approximated cubic fits of the data that is created by small linear approximations. Because of the nature of the fit, there is no explicit functional definition. Six separate splines are created; three each for translation and orientation. These splines can then be recombined to form a three-dimensional path which containing all precision points. A numerical example is shown in Figures 4-1, 4-2 and 4-3. In Figure 4-1, the desired path is shown along with the orientation at each pose. Figures 4-2 and 4-3 respectively show the values for translational and rotational components of each transformation at values for t computed using a weighting factor of $5^o = 0.6\ cm$. Values computed with the weighting factor are $t = \{0,\ 0.2957,\ 0.5130,\ 0.7826,\ 1\}$.

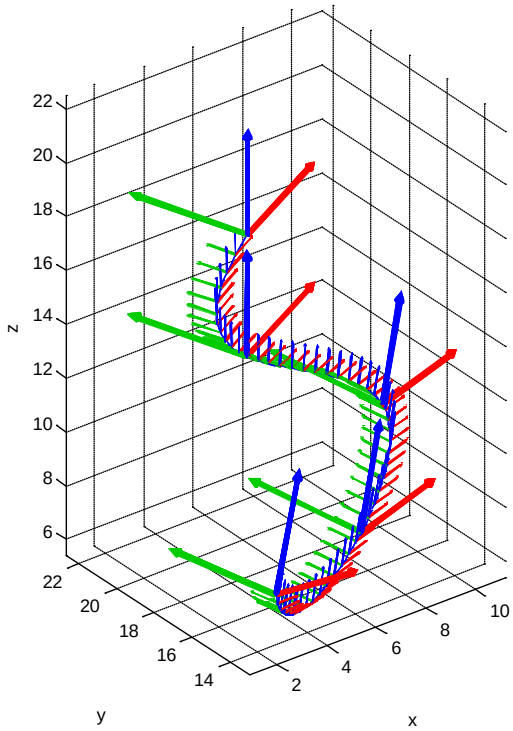

Figure 4-1. Example desired path.

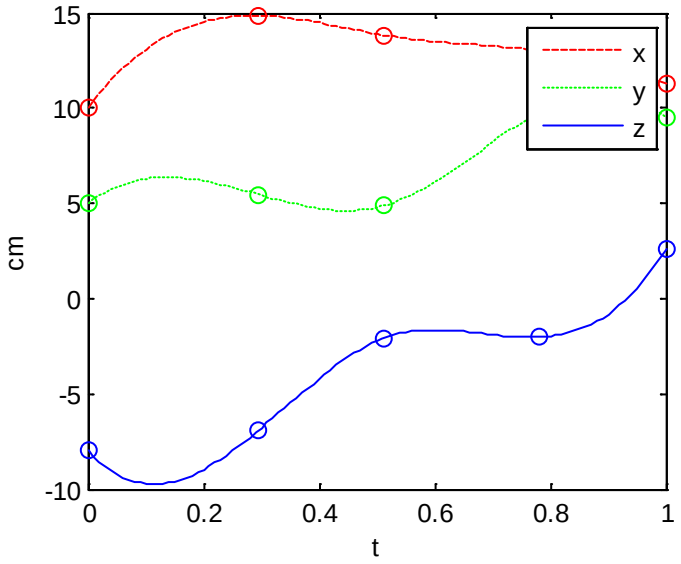

Figure 4-2. Example translational splines

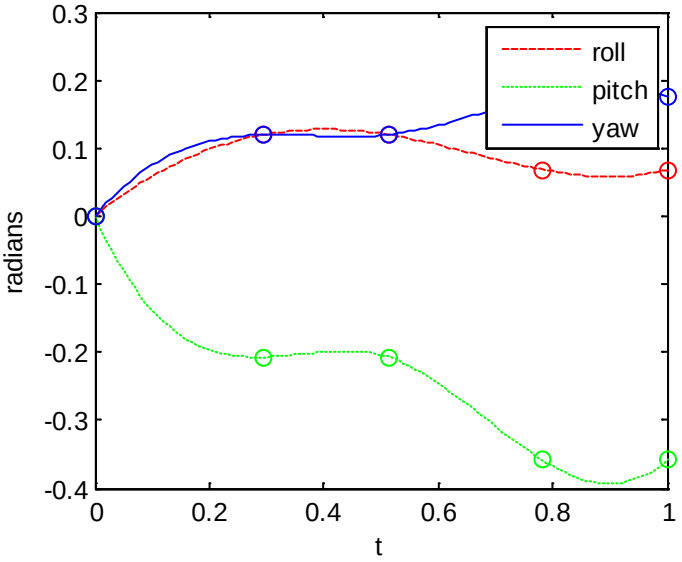

Figure 4-3. Example rotational splines

4.2 Scoring Function

A reverse kinematic analysis is performed at a series of one hundred evenly spaced points along the desired end effector path. This corresponds to $\Delta t = 0.1$ for the parameterized splines. This value provides balance between path resolution and computational time. At each point, a solution set is obtained that contains sixteen sets of joint angles that satisfy the specific position and orientation requirements. In general,

multiple sets of joint angles within a solution set will have nonzero imaginary values. These values indicate that the solution is in a configuration that is not physically attainable. This issue is addressed in Section 4.2.2.

An individual solution is chosen at the first point along the path. This defines the solution branch to be evaluated. For the given branch, a list of sequential joint angle values is composed. It is necessary to ensure that a single branch is used for an entire list of joint angles. If a set of joint angles does not belong to the branch of the preceding set, a discontinuity is experienced. The list of joint angles is stored in a 100×6 array such as in Equation 4-6.

$$\boldsymbol{\Theta} = \begin{bmatrix} {}_1\varphi_1 & {}_1\theta_2 & {}_1\theta_3 & {}_1\theta_4 & {}_1\theta_5 & {}_1\theta_6 \\ {}_2\varphi_1 & {}_2\theta_2 & {}_2\theta_3 & {}_2\theta_4 & {}_2\theta_5 & {}_2\theta_6 \\ \vdots & \vdots & \vdots & \vdots & \vdots & \vdots \\ {}_{100}\varphi_1 & {}_{100}\theta_2 & {}_{100}\theta_3 & {}_{100}\theta_4 & {}_{100}\theta_5 & {}_{100}\theta_6 \end{bmatrix} \tag{4-6}$$

A numerical derivative with respect to the length of the parameterized path (t) is taken of each column as in Equation 4-7. The numerical derivatives is found as a set of finite differences between joint angle values along the parameterized path

$$\omega_i = \frac{d\theta_i}{dt} \quad for\ \ i = 1 \ldots 6, \tag{4-7}$$

For a gear pair, the instantaneous gear ratio g can be defined as Equation 4-8.

$$g_n = \frac{\omega_{n+1}}{\omega_n} \quad for\ n = 1 \ldots 5 \tag{4-8}$$

A given set of gear profiles is scored as to how “circular” they are. A general circular gear has a constant gear ratio as in Equation 4-9.

$$\frac{dg}{dt} = 1 \tag{4-9}$$

The circularity of a given gear can therefore be evaluated by summing the magnitude of the differences in instantaneous gear ratio at adjacent points along the length of the path in Equation 4-10.

$$C'_n = \sum_{i=1}^{100} |\,_{i+1}g_n - \,_ig_n| \quad for\ n = 1 \dots 5 \tag{4-10}$$

The circularity score of each gear is summed with equal weighting to produce a scoring function for optimization in Equation 4-11.

$$S' = C'_1 + C'_2 + C'_3 + C'_4 + C'_5 \tag{4-11}$$

4.2.1 Imaginary Solutions

Non-reachable solutions characterized by imaginary joint angles must be excluded by a scoring function. However, complete exclusion creates sections of the design space with no gradient field, causing poor optimization performance. Therefore, sets of imaginary joint angles are not excluded, but are heavily penalized. The real and imaginary portions of the instantaneous gear ratio are split, and the imaginary part is scaled by a weighting factor (W_F) in order to drive down the magnitude of imaginary elements in Equation 4-12.

$$C_n = Re\{C'_n\} + W_F Im\{g_n\} \tag{4-12}$$

Setting the weighting factor many orders of magnitude greater than C'_n ensures a steep gradient, quickly excluding non-reachable solutions. Making this substitution, the scoring function becomes Equation 4-13.

$$S = C_1 + C_2 + C_3 + C_4 + C_5 \tag{4-13}$$

4.2.2 Singularities

For gear pair n, a mathematical singularity in the gear ratio occurs when $\omega_n = 0$ which causes g_n to approach infinity. This represents the case when one gear changes direction relative to the other. This is not physically viable, as these gears cannot be readily fabricated. The singularity causes sudden spikes in the value of the instantaneous gear ratio. These spikes heavily weigh the scoring function ($C_n^{'}$), providing a robust solution to designs that result in these singularities. Path resolution is chosen as to detect this singularity. The $\omega_n = 0$ solution is not found explicitly. Rather, the intermediate poses immediately preceding and following the direction change get close to $\omega_n = 0$, which results in large increases in the scoring function.

4.2.3 Limitations

This design algorithm provides a method for attaining non-circular gears to drive the mechanism through a desired path. However, due to the rigid method of path creation, many paths yield gear pairs that are not physically realizable. A design algorithm that solves this issue is presented in Chapter 5. Although not applicable to every desired path, this algorithm provides a straight-forward method of design and scoring for the open-loop geared spatial mechanism.

4.3 Numerical Example

A desired path is defined by six transformation matrices.

$$T_1^F = \begin{bmatrix} 0.2424 & 0.5198 & -0.8192 & -2.8388 \\ -0.9063 & 0.4226 & 0 & -10.3486 \\ 0.3462 & 0.7424 & 0.5736 & 6.3245 \\ 0 & 0 & 0 & 1 \end{bmatrix}$$

$$T_2^F = \begin{bmatrix} -0.1794 & 0.6525 & -0.7362 & -6.9302 \\ -9.208 & 0.1520 & 0.3591 & -6.8499 \\ 0.3462 & 0.7424 & 0.5736 & 6.6232 \\ 0 & 0 & 0 & 1 \end{bmatrix}$$

$$T_3^F = \begin{bmatrix} -0.5649 & 0.6531 & -0.5043 & -9.3051 \\ -0.7490 & -0.1494 & 0.6455 & -1.7943 \\ 0.3462 & 0.7424 & 0.5736 & 6.9446 \\ 0 & 0 & 0 & 1 \end{bmatrix}$$

$$T_4^F = \begin{bmatrix} -0.8361 & 0.5215 & -0.1703 & -9.3935 \\ -0.4255 & -0.4206 & 0.8013 & 3.9446 \\ 0.3462 & 0.7424 & 0.5736 & 7.2861 \\ 0 & 0 & 0 & 1 \end{bmatrix}$$

$$T_5^F = \begin{bmatrix} -0.9380 & 0.2843 & 0.1982 & -7.0530 \\ -0.0159 & -0.6066 & -0.7948 & 9.2959 \\ 0.3462 & 0.7424 & 0.5736 & 7.6451 \\ 0 & 0 & 0 & 1 \end{bmatrix}$$

$$T_6^F = \begin{bmatrix} -0.9176 & 0.1406 & 0.3719 & -5.0519 \\ 0.1955 & -0.6550 & 0.7299 & 11.4881 \\ 0.3462 & 0.7424 & 0.5736 & 7.8303 \\ 0 & 0 & 0 & 1 \end{bmatrix}$$

A flow chart of the design algorithm is shown in Figure 4-4. Each transformation matrix can be broken into three translation and three rotational components which is expanded by a spline fit. A mapping metric is used such that five degrees equals 0.6 centimeters. The splines are defined by a variable *t* which varies from 0 to1. When $t = 0$ the splines evaluate to the first end effector pose along the path. When $t = 1$ the splines evaluate to the last on pose the path. The spline values are presented in Table 4-1. The complete path is shown in Figure 4-5. In the graphs below (Figure 4-6, Figure 4-7), open circles represent the location of precision points.

Dimensional optimization is performed with this desired path. Optimization is bounded as in Table 4-2. Diversity is controlled by the initial range of the initial population, which is set as in Table 4-3. The genetic algorithm optimization is run ten times, and the best score is obtained with the parameters listed in Table 4-4.

Quasi-Newton optimization is then performed using the bounds from Table 4-2. The genetic algorithm optimization results from Table 4-4 are used as the initial guess.

The results of the Quasi-Newton optimization are summarized in Table 4-5. The Quasi-Newton optimization provides a dimensional solution resulting in continuous, smooth non-circular gears. Angular position values for each joint are displayed in Figure 4-8 for each point at which the reverse kinematic analysis is performed. The instantaneous gear ratios ($g_n : 1$) are displayed in Figure 4-9 for each reverse analysis point. Input/Output plots for individual gear pairs are displayed in Figure 4-10.

Table 4-1. Spline parameters

Pose	Parameter	Roll (rad)	Pitch (rad)	Yaw (rad)	X (cm)	Y (cm)	Z (cm)
1	0	0.0000	-0.9559	-1.1345	-2.8388	-10.3486	6.3245
2	0.2150	-0.5594	-0.8275	-1.8392	-6.9302	-6.8499	6.6232
3	0.4351	-0.8443	-0.5286	-2.2840	-9.3051	-1.7943	6.9446
4	0.6591	-0.9495	-0.1711	-2.5839	-9.3935	3.9446	7.2861
5	0.8857	-0.9457	0.1995	-2.8473	-7.0530	9.2959	7.6451
6	1	-0.9407	0.3810	-2.9896	-5.0619	11.4881	7.8303

Table 4-2. Dimensional bounds

Offset distance (cm)	Link lengths (cm)	Twist angles (degrees)
$S_2 = [0.1, 20]$	$a_{12} = [0.1, 20]$	$\alpha_{12} = 0$
$S_3 = 0$	$a_{23} = 0$	$\alpha_{23} = [0.1, 280]$
$S_4 = [0.1, 20]$	$a_{34} = [0.1, 20]$	$\alpha_{34} = 0$
$S_5 = 0$	$a_{45} = 0$	$\alpha_{45} = [0.1, 280]$
$S_6 = [0.1, 20]$	$a_{56} = [0.1, 20]$	$\alpha_{56} = 0$

Table 4-3. Initial population range for genetic algorithm optimization

Offset distance (cm)	Link lengths (cm)	Twist angles (degrees)
$S_2 = [3, 8]$	$a_{12} = [1, 6]$	$\alpha_{12} = 0$
$S_3 = 0$	$a_{23} = 0$	$\alpha_{23} = [70, 120]$
$S_4 = [4, 13]$	$a_{34} = [1, 6]$	$\alpha_{34} = 0$
$S_5 = 0$	$a_{45} = 0$	$\alpha_{45} = [70, 120]$
$S_6 = [6, 11]$	$a_{56} = [2, 7]$	$\alpha_{56} = 0$

Table 4-4. Genetic algorithm results

Offset distance (cm)	Link lengths (cm)	Twist angles (degrees)
$S_2 = 7.2729$	$a_{12} = 9.9995$	$\alpha_{12} = 0$
$S_3 = 0$	$a_{23} = 0$	$\alpha_{23} = 130.9404$
$S_4 = 13.8577$	$a_{34} = 8.7209$	$\alpha_{34} = 0$
$S_5 = 0$	$a_{45} = 0$	$\alpha_{45} = 118.9175$
$S_6 = 14.1003$	$a_{56} = 9.9978$	$\alpha_{56} = 0$
$\text{branch} = 4, \text{score} = 1.9586$		

Table 4-5. Quasi-newton results

Offset distance (cm)	Link lengths (cm)	Twist angles (degrees)
$S_2 = 0.1731$	$a_{12} = 18.9506$	$\alpha_{12} = 0$
$S_3 = 0$	$a_{23} = 0$	$\alpha_{23} = 136.8717$
$S_4 = 8.1420$	$a_{34} = 15.8695$	$\alpha_{34} = 0$
$S_5 = 0$	$a_{45} = 0$	$\alpha_{45} = 118.2651$
$S_6 = 14.2196$	$a_{56} = 19.4163$	$\alpha_{56} = 0$
$\text{branch} = 4\,, \text{score} = 1.2238$		

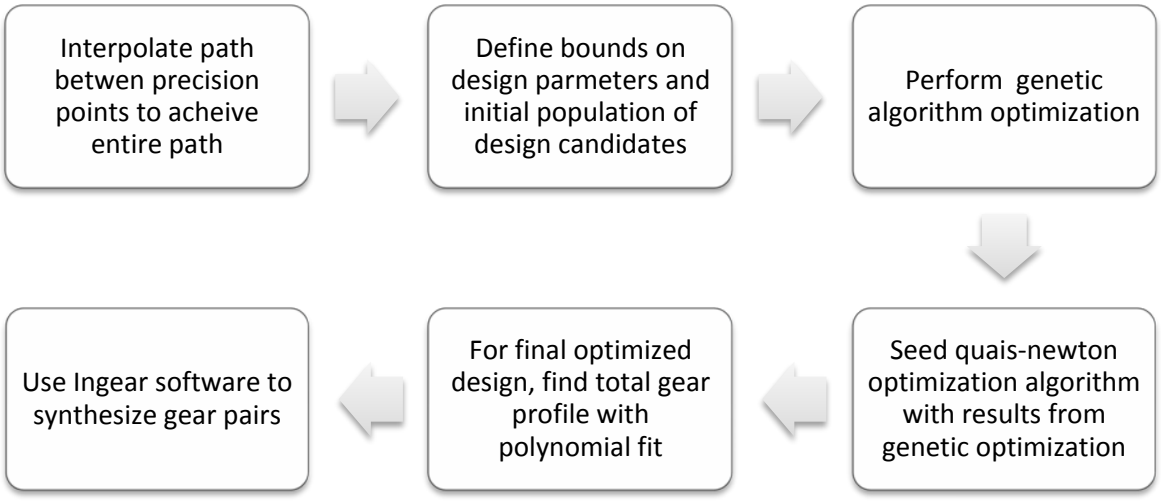

Figure 4-4. Flow chart of design algorithm

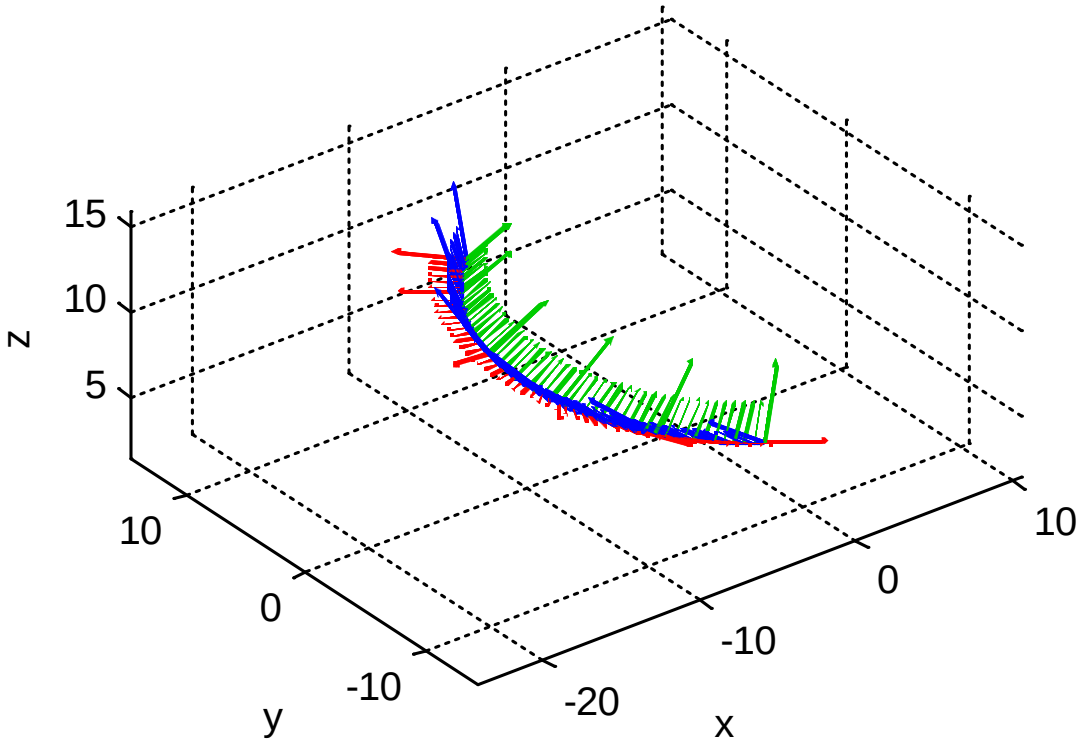

Figure 4-5. Three dimensional desired path (cm).

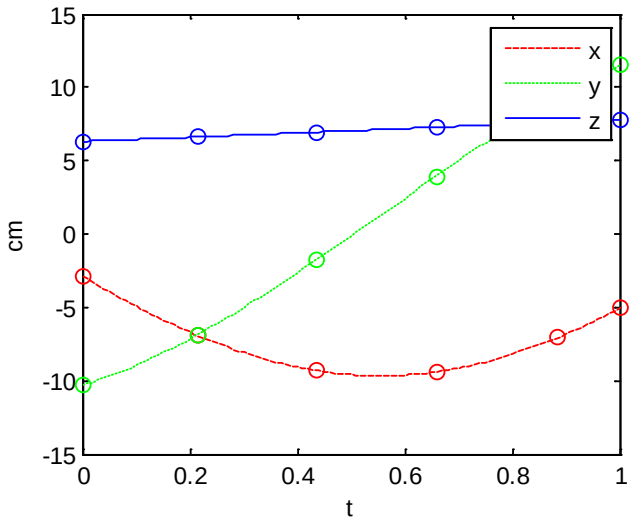

Figure 4-6. X/Y/Z coordinates of tool point for spline t.

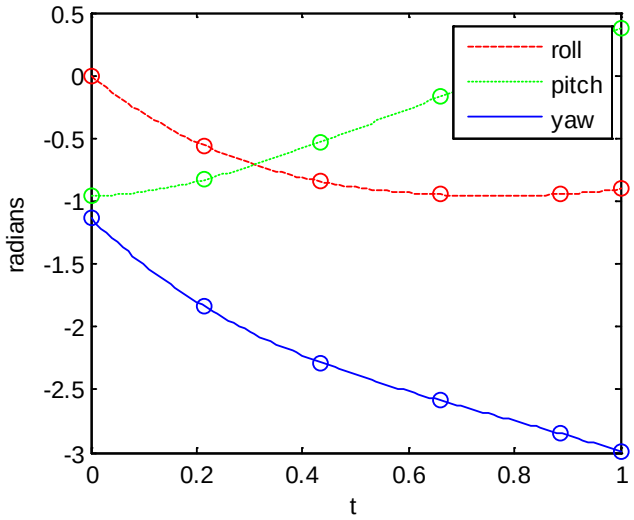

Figure 4-7. Roll/pitch/yaw angles for spline t.

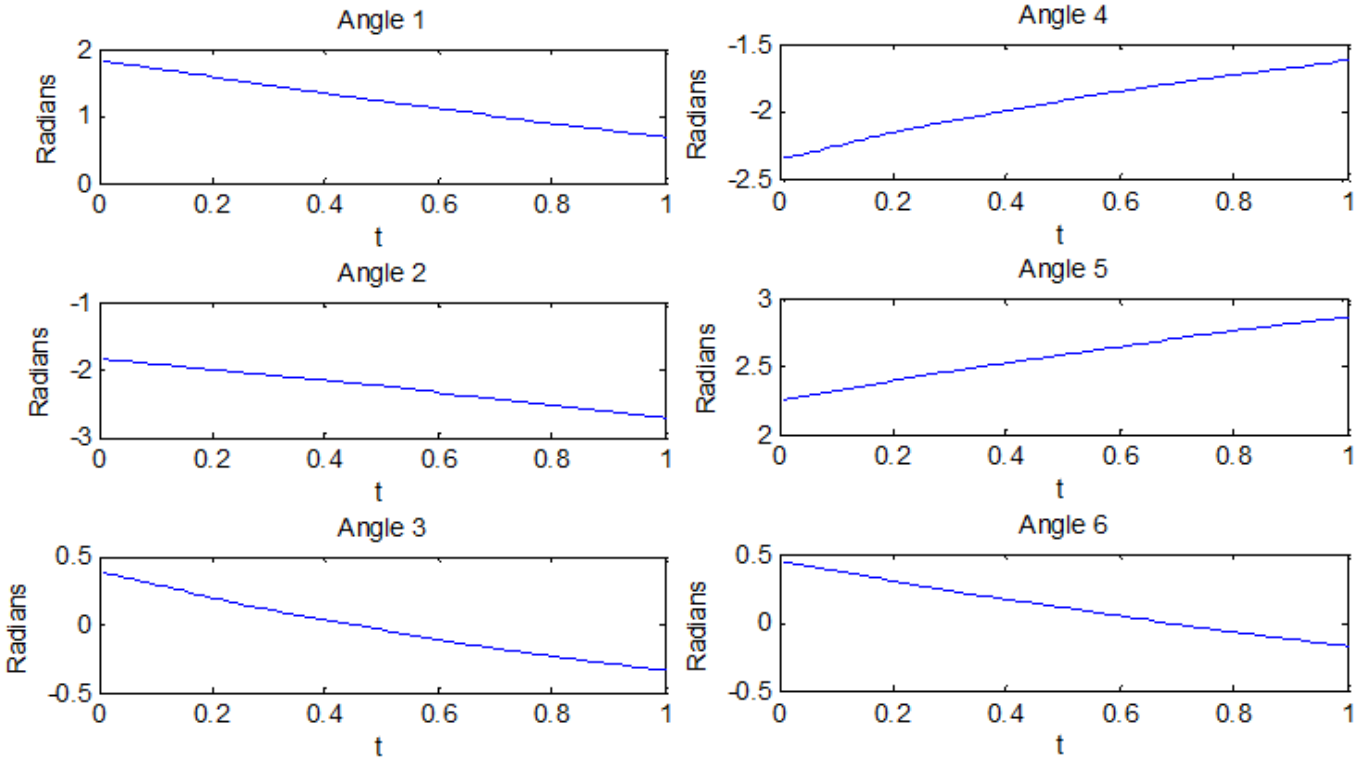

Figure 4-8. Angular positions of joints

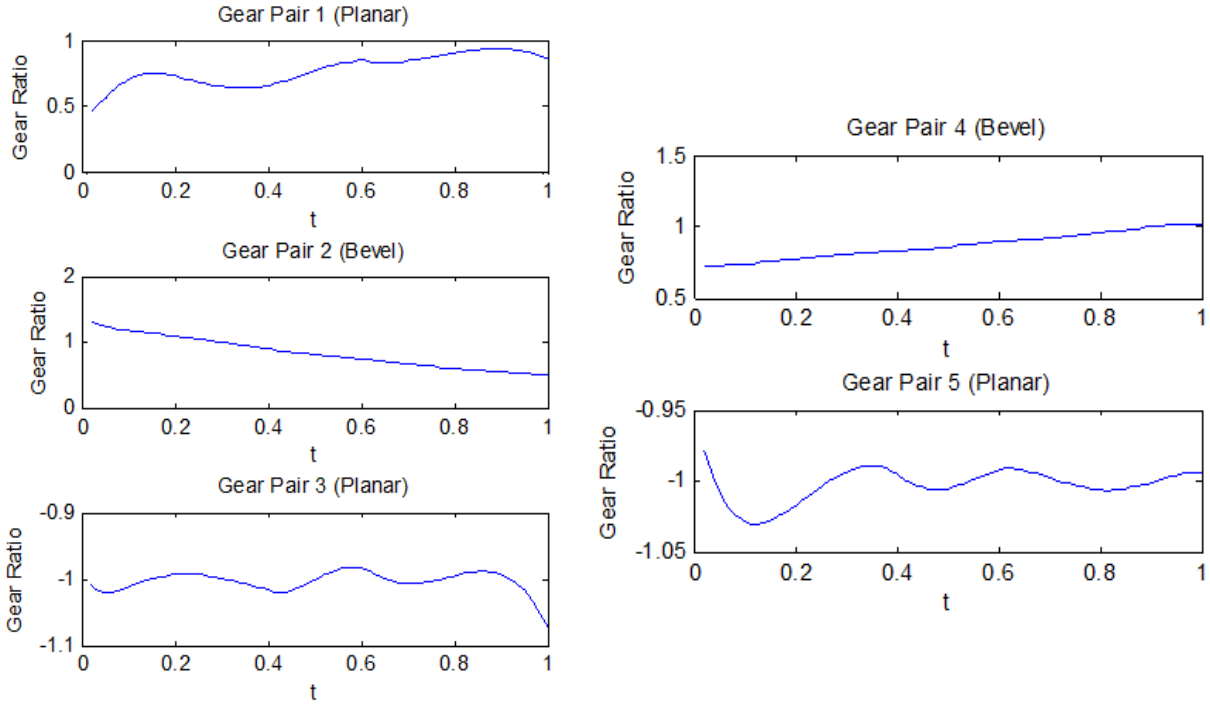

Figure 4-9. Instantaneous gear ratios

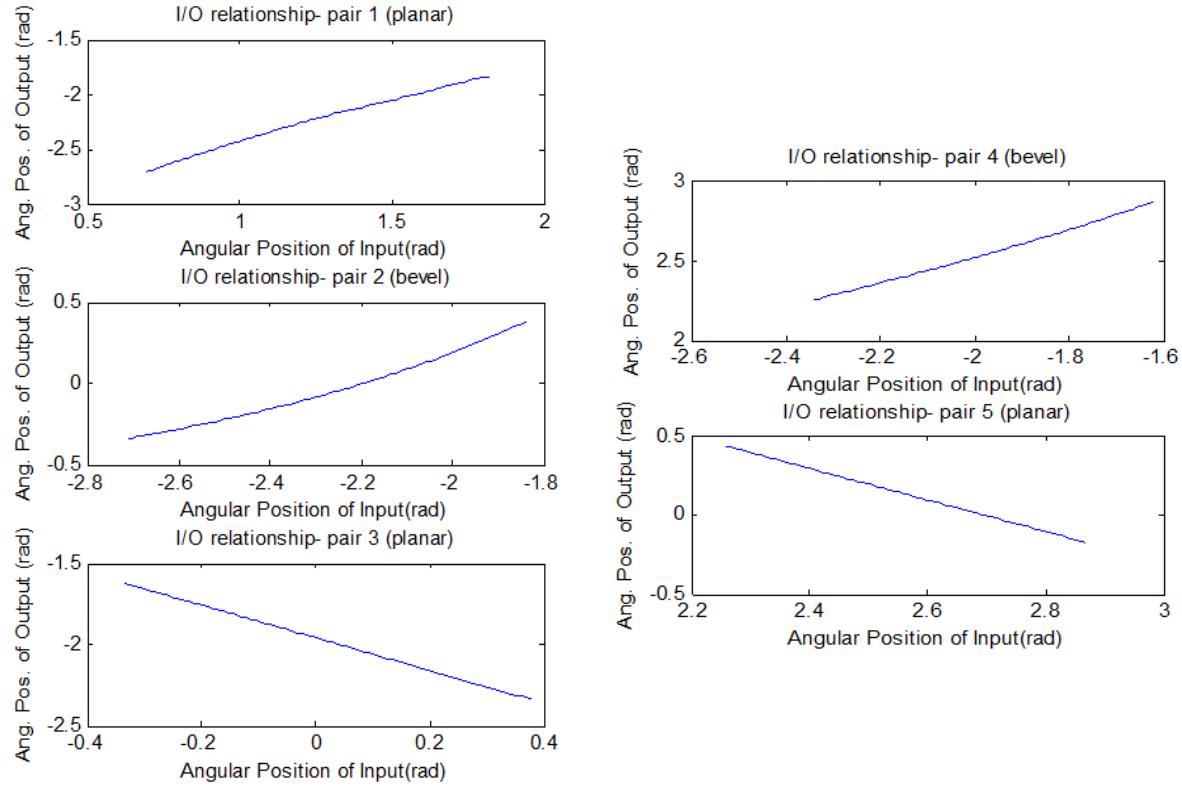

Figure 4-10. Input/output plots

CHAPTER 5
PRECISON POINT SYNTHESIS

5.1 Path Creation

In the precision point design synthesis, a path is again defined by a set of desired positions and orientations of the end effector named precision points. For precision point synthesis, roll, pitch and yaw angles as well as X, Y and Z coordinates of the base with respect to the path is included in the parameter set. Equations 4-2 to 4-5 describe how these angles are converted to an initial transformation matrix from the first pose to the fixed reference frame. Subsequent poses are defined by a series of translations and rotations from the first pose. In this manner, altering the first transformation matrix moves the entire path with respect to the fixed reference frame. This allows for the optimization of the position and orientation of the base as well as the link lengths, joint offsets and twist angles.

Reverse analysis is performed on each precision point defined by a transformation matrix for a given candidate set of optimization parameters. The reverse kinematic analysis produces sixteen sets of joint angles for the given set of mechanism parameters.

A solution branch is selected and an ordered list of angles is compiled for each joint angle ($\varphi_1, \theta_2, \theta_3, \theta_4, \theta_5, \theta_6$). For each joint angle list, a relative angular displacement is computed. This angular displacement is normalized as the basis for a spline fit used to create the joint angles for each point along the path between precision points. The forward kinematic analysis is performed with the computed joint angles and the candidate mechanism parameters to create the transformation matrix at each point.

This path creation algorithm allows a greater degree of design flexibility when compared to the algorithm described in Chapter 4. The path between precision points is defined by the candidate set of parameters and is not constricted beforehand. Since the path is not defined outside of the precision points, there exist far fewer limiting points on the path, increasing the likelihood of a physically viable solution.

5.2 Scoring Function

With the precision point design algorithm, the joint angle array defined by Equation 4-6 is given by the splines produced by the joint angles at precision points. This eliminates the need to perform reverse analysis at each point along the path. This reduces the computational time by greater than an order of magnitude when compared to the exact path specification algorithm. A comparative test showed a decrease in optimization time from over seventeen hours to just over twenty-three minutes for a large-scale optimization problem with five specified positions and orientations

The flexibility in the path necessitates more constraints on the scoring function. Gear motion direction changes and intra-gear pair relative motion direction changes must be explicitly penalized. The number of times that a given gear pair (V_Δ) changes directions is computed by counting the number of times that the instantaneous kinematic velocity of the output gear with respect to the input gear changes from positive to negative or negative to positive. The number of times that the gear pairs change direction relative to each other (P_Δ) is computed by counting the number of times that the plot of the output angle changes directions relative to path parameter. These counts are weighted (W_v, W_p) and summed as in Equation 5-1.

$$D_n = W_v * V_\Delta + W_p * P_\Delta \quad for\ n = 1, \dots, 5 \qquad (5-1)$$

The circularity of a given gear pair is scored by summing the deviance of the instantaneous gear ratio defined in Equations 4-7 and 4-8 from the gear ratio of 1 over the entire path as in Equation 5-2. This circularity score differs slightly from that used in Chapter 4. Both scores effectively grade the circularity of the gear pair, but the earlier circularity equation has a floating reference point from which the deviance is calculated. Equation 5-2 uses the gear ratio 1 as the absolute reference point. This eliminates the possibility of a gradual increase of the gear ratio without penalty. This change also penalizes gear pairs with a net ratio that is not 1. For non-circular gears, the net ratio is chosen at 1 to ensure that every input revolution results in a single output revolution.

$$C_n^{'} = \sum_{i=1}^{100} |1 - g_i| \quad for\ n = 1 \dots 5 \tag{5-2}$$

Again, the scoring function must compensate for imaginary solutions as in Equation 5-3. The imaginary portion is weighted heavily to quickly drive the scoring function out of imaginary regions.

$$C_n = Re\{C^{'}{}_n\} + W_F Im\{g_n\} \tag{5-3}$$

The total circularity score of the candidate design is found by summing the circularity scores for individual gear pairs with a weighting factor as Equation 5-4.

$$C = W_C(C_1 + C_2 + C_3 + C_4 + C_5) \tag{5-4}$$

In order to ensure gear continuity, the kinematic acceleration of the gear pair is computed and penalized. The angular acceleration of each gear is computed by Equation 5-5.

$$\alpha_i = \frac{d\omega_i}{dt} \quad for\ \ i = 1 \dots 6 \tag{5-5}$$

The kinematic acceleration of the gear pair is then defined by Equation 5-6. The complete kinematic acceleration score is created by summing the acceleration scores of the gear pairs with a weighting factor as in Equation 5-7.

$$A_n = \frac{\alpha_{n+1}}{\alpha_n} \quad for\ n = 1 \ldots 5 \tag{5-6}$$

$$A = W_A(A_1 + A_2 + A_3 + A_4 + A_5) \tag{5-7}$$

The total score for a candidate design is created by summing all of the scoring components and their weights in Equation 5-8.

$$S = D + C + A \tag{5-8}$$

This scoring function provides robustness against imaginary solutions and singularities. This is largely a function of the circularity score. The other aspects of the scoring function serve to guide the optimization towards a more physically attainable solution.

5.3 Numerical Example

A desired path is defined by the following translations and roll, pitch and yaw angles relative to the candidate first pose.

${}^{2}_{1}T$ is produced by translating the ${}^{1}_{F}T$ along the vector $\begin{bmatrix} -4.4048 \\ 3.7189 \\ 4.5084 \end{bmatrix}$ cm with

$roll = -0.5608$, $pitch = -0.1874$, $yaw = -0.5327$ radians.

${}^{3}_{2}T$ is produced by translating the ${}^{2}_{1}T$ along the vector $\begin{bmatrix} -10.0589 \\ 3.3143 \\ 4.0983 \end{bmatrix}$ cm with

$roll = -1.1386$, $pitch = 0.4502$, $yaw = 3.1335$ radians.

${}^{4}_{3}T$ is produced by translating the ${}^{3}_{2}T$ along the vector $\begin{bmatrix} -21.3910 \\ -1.6621 \\ -12.4279 \end{bmatrix}$ cm with

$roll = -1.9983, pitch = -0.0843, yaw = -2.7088$ radians.

${}^{5}_{4}T$ is produced by translating the ${}^{4}_{3}T$ along the vector $\begin{bmatrix} -0.4276 \\ -22.5314 \\ -9.4250 \end{bmatrix}$ cm with

$roll = 0.9918, pitch = -0.1168, yaw = -0.3558$ radians.

${}^{6}_{5}T$ is produced by translating the ${}^{4}_{5}T$ along the vector $\begin{bmatrix} 21.3244 \\ 3.9853 \\ -2.3050 \end{bmatrix}$ cm with

$roll = -0.7752, pitch = 0.7008, yaw = -0.0588$ radians.

The genetic algorithm optimization is run 20 times with the desired path. Repeated optimizations are necessitated by the random nature of the genetic algorithm. A different set of initial candidate solutions, or even a chance parametric mutation, can cause the algorithm to fail. Bounds are set on the design space as defined in Table 5-1. The genetic algorithm is seeded within the initial population defined in Table 5-2. The initial population is specified in order to lead the search algorithm towards a solution with desirable features such as low link length to joint offset ratio and twist angles close to 90 degrees.

Because the genetic algorithm does no directed searching, there is no reason to believe that the candidate parameters result in an absolute minimum of the scoring function. Therefore, the quasi-Newton algorithm is utilized to ensure the best solution possible. The results of the genetic algorithm optimization highlighted in Table 5-3 serve as the starting point for this search. The results of the quasi-Newton search are presented in Table 5-4. Joint angle plots are displayed in Figure 5-1. The joint angles at precision points are marked by open circles. The position and orientation of the first pose result in the initial transformation matrix about which all other poses are based.

The transformation matrix of pose i is defined as T_i^F. The transformation matrices for the desired path are listed below.

$$T_1^F = \begin{bmatrix} 0.9216 & 0.0676 & 0.3822 & 20.0000 \\ -0.3772 & -0.0758 & 0.9230 & 10.3754 \\ 0.0913 & -0.9948 & -0.0444 & 14.6198 \\ 0 & 0 & 0 & 1 \end{bmatrix}$$

$$T_2^F = \begin{bmatrix} 0.9471 & -0.3206 & -0.0127 & 15.5952 \\ 0.1311 & 0.3507 & 0.9273 & 14.0943 \\ -0.2929 & -0.8799 & 0.3742 & 19.1282 \\ 0 & 0 & 0 & 1 \end{bmatrix}$$

$$T_3^F = \begin{bmatrix} -0.8517 & 0.2744 & 0.4465 & 5.5363 \\ -0.3277 & -0.9437 & -0.0451 & 17.4086 \\ 0.4090 & -0.1848 & 0.8937 & 23.2265 \\ 0 & 0 & 0 & 1 \end{bmatrix}$$

$$T_4^F = \begin{bmatrix} 0.9053 & -0.4230 & -0.0392 & -15.8356 \\ -0.1579 & -0.4208 & 0.8933 & 15.7465 \\ -0.3943 & -0.8025 & -0.4478 & 10.7986 \\ 0 & 0 & 0 & 1 \end{bmatrix}$$

$$T_5^F = \begin{bmatrix} 0.9788 & -0.0891 & -0.1846 & -16.2632 \\ -0.0806 & -0.9953 & 0.0530 & -6.7849 \\ -0.1885 & -0.0370 & -0.9814 & 1.3736 \\ 0 & 0 & 0 & 1 \end{bmatrix}$$

$$T_6^F = \begin{bmatrix} 0.8654 & 0.4377 & 0.2439 & 5.0612 \\ 0.1254 & -0.6605 & 0.7403 & -2.7996 \\ 0.4851 & -0.6101 & -0.6265 & -0.9314 \\ 0 & 0 & 0 & 1 \end{bmatrix}$$

This path is displayed in Figure 5-2. The path initially rises and maintains a steady orientation path. At the top of the path, the orientation of the end effector begins to rapidly rotate and the position drops vertically and in one horizontal direction. At the end of the path, the end effector maintains elevation and moves largely in the horizontal plane. This arbitrary path has a wide variety of uses including precision welding of highly non-linear surfaces and product pick and place.

The kinematic velocity of each gear pair is displayed in Figure 5-3. The instantaneous kinematic velocity is the same as the gear ratio $(g_n{:}\,1)$ as in Figure 4-5. The kinematic velocities are extended to form the kinematic velocity plot for an entire non-circular gear pair with net ratio of 1:1. The non-active portion of the gear is specified in the velocity domain by Dooner (2001) and is formed by fitting the polynomial with respect to input angle in Equation 5-9 subject to the constraints defined in Equation 5-10. The position, angular velocity and angular acceleration of the output with respect to the input at the last pose are denoted by θ_f, ω_f and α_f, respectively. The angular velocity and angular acceleration at the first pose are specified as ω_o and α_o. The end points of the polynomial are defined as P_1 and P_2.

$$P(\theta_i) = a_4\theta_i^4 + a_3\theta_i^3 + a_2\theta_i^2 + a_1\theta_i + a_0 \qquad (5-9)$$

$$P_1 = \omega_f$$

$$P_1^{'} = \alpha_f$$

$$P_2 = \omega_o \qquad (5-10)$$

$$P_2^{'} = \alpha_o$$

$$\int_0^{\theta_f} \omega_i(\theta_i)d\theta_i + \int_{\theta_f}^{2\pi} P(\theta_i)d\theta_i = 2\pi$$

In Figure 5-3, the solid line represents the active portion of the gear while the dashed line is the polynomial resulting from Equations 5-9 and 5-10.

The kinematic velocity data for the complete gear is input into the INGEAR software. The software provides a robust method for the development of generalized gears. It is particularly potent for the creation of non-circular gears. Screw theory methods are used to create physical gears for a desired trajectory and parameter set.

Stereolithography files are generated and used to create prototype gears. An example of the gears produced for gear pair 2 is shown below in Figure 5-4. The gears have a shaft angle dictated by α_{23}. The input gear is on the right and the gears are shown in mesh at pose 1.

Table 5-1. Dimensional bounds

Offset distance (cm)	Link lengths (cm)	Twist angles (degrees)	Position of base (cm)	Orientation of base (degrees)
$S_2 = [2, 20]$	$a_{12} = [2,20]$	$\alpha_{12} = 0$	X = [-20,20]	Roll = [0,359]
$S_3 = 0$	$a_{23} = 0$	$\alpha_{23} = [0,359]$	Y = [-20,20]	Pitch = [0,359]
$S_4 = [2, 20]$	$a_{34} = [2,20]$	$\alpha_{34} = 0$	Z = [-20,20]	Yaw = [0,359]
$S_5 = 0$	$a_{45} = 0$	$\alpha_{45} = [0,359]$		
$S_6 = [2, 20]$	$a_{56} = [2,20]$	$\alpha_{56} = 0$		

Table 5-2. Initial population range for genetic algorithm optimization

Offset distance (cm)	Link lengths (cm)	Twist angles (degrees)	Position of base (cm)	Orientation of base (degrees)
$S_2 = [9,12]$	$a_{12} = [3,6]$	$\alpha_{12} = 0$	X = [18,20]	Roll = [90,180]
$S_3 = 0$	$a_{23} = 0$	$\alpha_{23} = [80,110]$	Y = [9,11]	Pitch = [0,90]
$S_4 = [9,12]$	$a_{34} = [3,6]$	$\alpha_{34} = 0$	Z = [14,16]	Yaw = [0,90]
$S_5 = 0$	$a_{45} = 0$	$\alpha_{45} = [80,110]$		
$S_6 = [9,12]$	$a_{56} = [3,6]$	$\alpha_{56} = 0$		

Table 5-3. Genetic algorithm results

Offset distance (cm)	Link lengths (cm)	Twist angles (degrees)	Position of base (cm)	Orientation of base (degrees)
$S_2 = 8.5948$	$a_{12} = 4.3935$	$\alpha_{12} = 0$	X = 19.7491	Roll = 265.9640
$S_3 = 0$	$a_{23} = 0$	$\alpha_{23} = 88.3247$	Y = 10.4973	Pitch = 25.1538
$S_4 = 9.5908$	$a_{34} = 4.5661$	$\alpha_{34} = 0$	Z = 13.8915	Yaw = 346.5936
$S_5 = 0$	$a_{45} = 0$	$\alpha_{45} = 91.8139$		
$S_6 = 11.6491$	$a_{56} = 4.5379$	$\alpha_{56} = 0$		
$\text{branch} = 16, \text{score} = 233.5577$				

Table 5-4. Quasi-newton results

Offset distance (cm)	Link lengths (cm)	Twist angles (degrees)	Position of base (cm)	Orientation of base (degrees)
$S_2 = 9.1246$	$a_{12} = 3.3398$	$\alpha_{12} = 0$	X = 20	Roll = 267.2457
$S_3 = 0$	$a_{23} = 0$	$\alpha_{23} = 88.3247$	Y = 10.3753	Pitch = 22.4679
$S_4 = 9.8750$	$a_{34} = 4.1289$	$\alpha_{34} = 0$	Z = 14.6198	Yaw = 355.8072
$S_5 = 0$	$a_{45} = 0$	$\alpha_{45} = 91.8139$		
$S_6 = 10.9394$	$a_{56} = 4.8051$	$\alpha_{56} = 0$		
$\text{branch} = 16, \text{score} = 109.4138$				

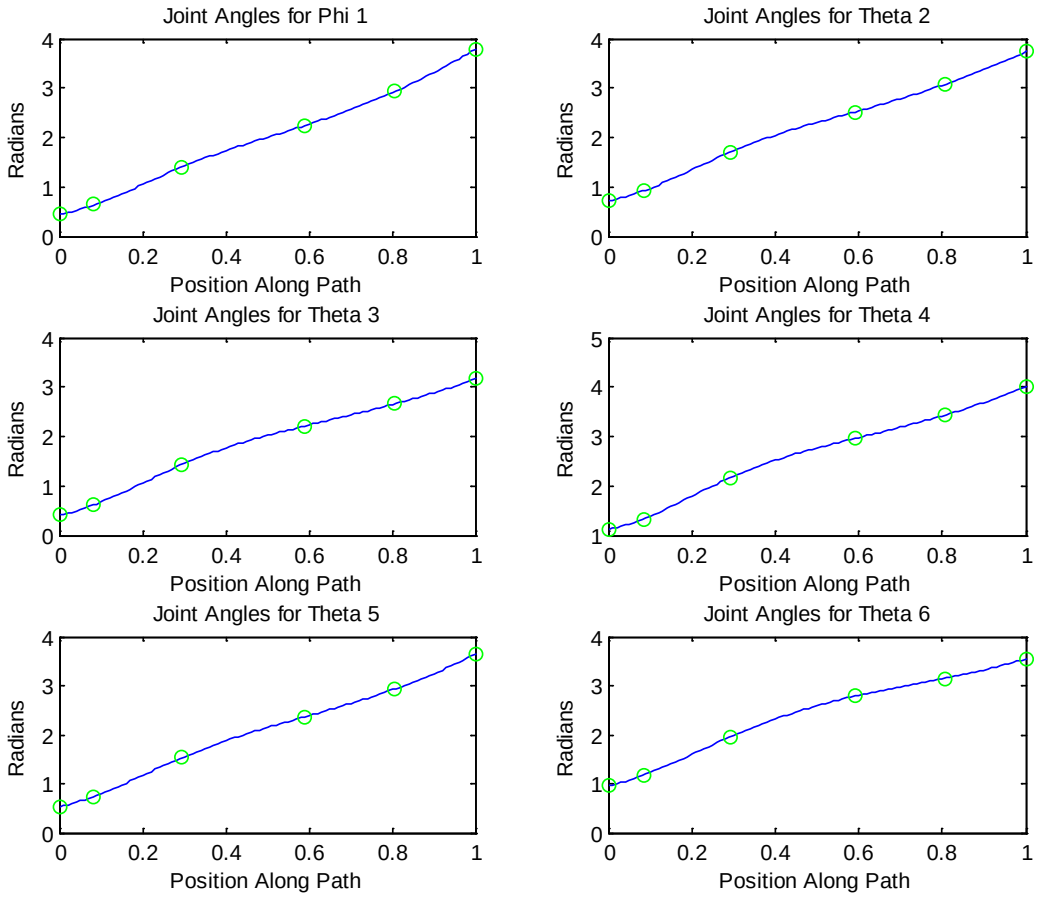

Figure 5-1. Joint angles for precision point synthesis numerical example

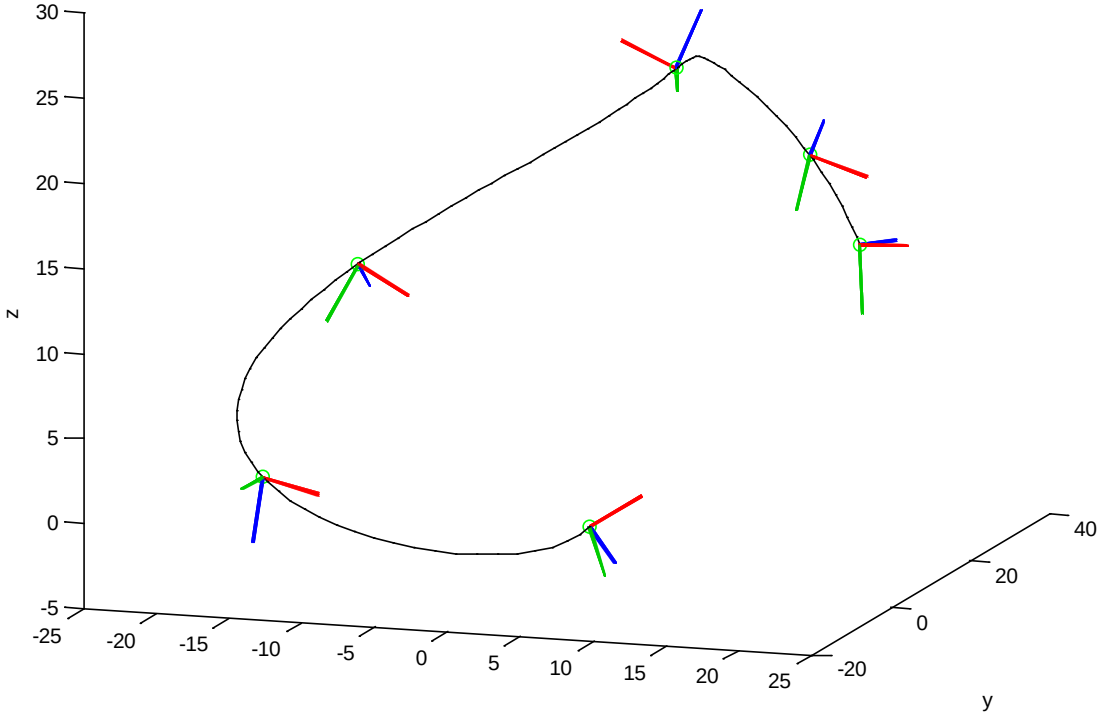

Figure 5-2. Path traced by end effector

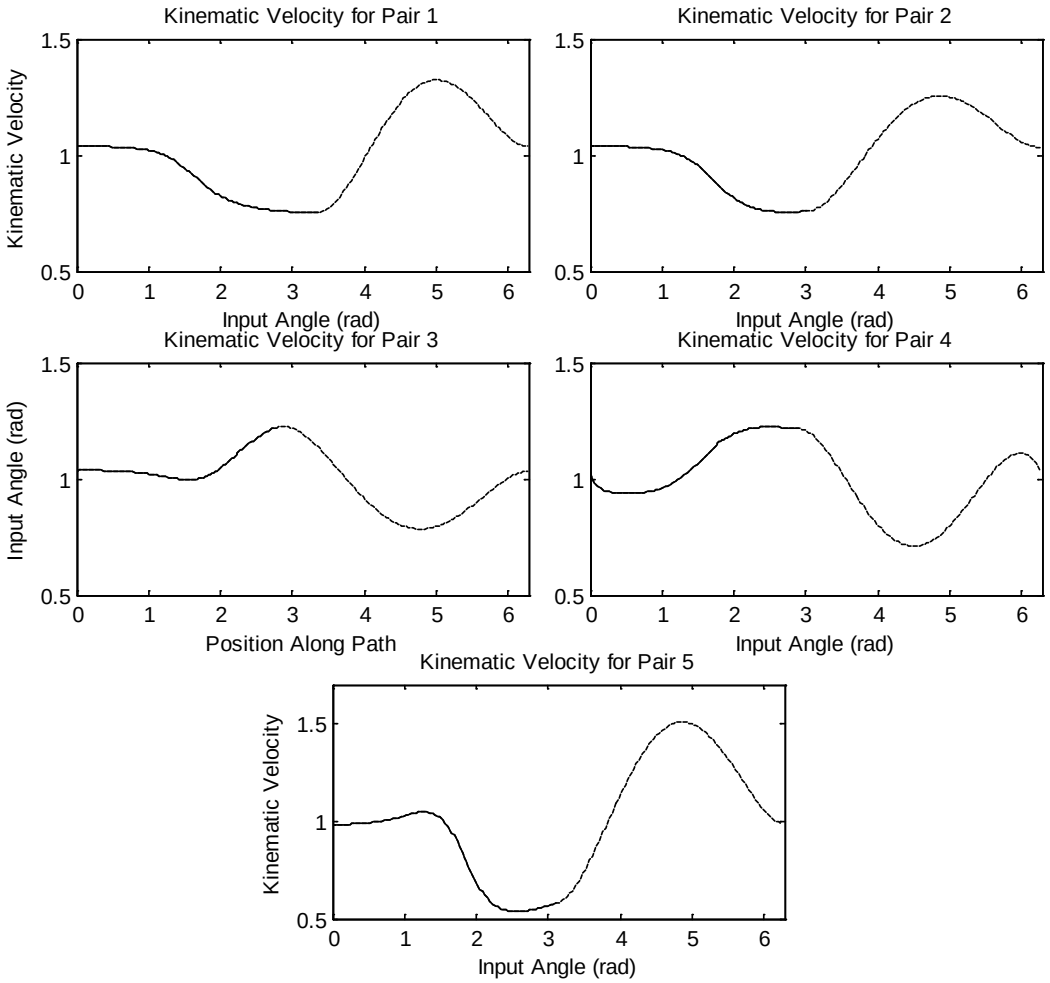

Figure 5-3. Kinematic velocities for numerical example

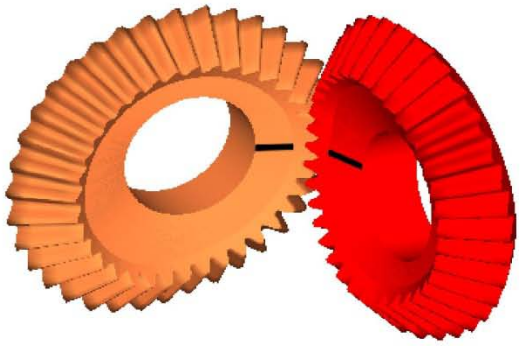

Figure 5-4. Gear pair produced by Ingear software

CHAPTER 6
CONCLUSION

Two algorithms are presented for the design of a single degree of freedom open-loop spatial manipulator with a special geometry that allows for the use of geared connections to control end effector movement. The first algorithm utilizes an exact desired path for the end effector. Gears are scored on their degree of “circularity”. A candidate design including joint offset, link length and twist angle parameters is optimized to create circular gears. This algorithm succeeds, but is limited in use due to the high degree of nonlinearity in the system and strict path adherence.

A second algorithm is presented that generates a path that is flexible for a candidate design. The path is defined by an ordered series of desired positions and orientations. The desired poses are termed “precision points”. The end effector motion between the precision points is not constrained, allowing a greater ability to provide realistic non-circular gears for any generalized path. The precision point algorithm necessitates that the gears of a candidate design must be scored not only on circularity but also on absolute and relative motion directionality. Physically viable gears are designed and created using Ingear.

Future work for this project includes dynamic force analysis including the identification of reaction loads and link balancing. These are necessary next steps to the broad realization of single degree of freedom open-loop mechanisms in industry. Further path definition including velocity constraints on precision points is another area of exploration for this work. A driving mechanism to link a constant torque motor to the first link must also be developed. A closed-loop single degree of freedom manipulator is also under investigation.

LIST OF REFERENCES

Crane, C., and Duffy, J. (1998). *Kinematic Analysis of Robot Manipulators*, Cambridge University Press.

Danieli, G. A., and Mundo, D. (2004). "New Developments in Variable Radius Gears Using Constant Pressure Angle Teeth." *Mechanism and Machine Theory*, 40, 203-217.

Dooner, D., and Seireg, A. (1995). *The Kinematic Geometry of Gearing; A Concurrent Engineering Approach*, John Wiley, New York.

Dooner, D. B. (2001). "Function generation utilizing an eight-link mechanism and optimized non-circular gear elements with application to automotive steering." *Proceedings of the Insititution of Mechanical Engineers*, 847-857.

Dou, X., and Ting, K.-L. (1996). "Branch Identification of Geared Five-Bar Chains." *Journal of Mechanical Design*, 118, 384-389.

Duffy, J., and Rooney, J. (1975). "A foundation for a unified theory of analysis of spatial mechanisms." *ASME J. Eng. Ind.*, 97B(4), 1159-1164.

Harshe, M. (2009). "Design of One Degree of Freedom Closed Loop Spatial Chains Using Non-Circular Gears," University of Florida, Gainesville, FL.

Krovi, V., Ananthasuresh, G. K., and Kumar, V. (2002). "Kinematic and kinetostatic synthesis of planar coupled serial chain mechanisms." *Journal of Mechanical Design, Transactions of the ASME*, 124(2), 301-312.

McKinley, J. R., Crane, C., and Dooner, D. (2007). "Reverse Kinematic Analysis of the Spatial Six Axis Robotic Manipulator with Consecutive Joint Axes Parallel." *ASME International Design Engineering Technical Conferences and Computers and Information in Engineering Conference*, Las Vegas, NV.

McKinley, J. R., Crane, C., and Dooner, D. (2008). "Three-dimensional rigid body guidance using gear connections in a robotic manipulator with parallel consectuive axes." *ASME Design Engineering Technical Conferences*, New York, NY.

Modler, K. H., Lovasz, E. C., Bar, G. F., Neumann, R., Perju, D., Perner, M., and Margineanu, D. (2009). "General method for the synthesis of geared linkages with non-circular gears." *Mechanism and Machine Theory*, 44(4), 726-738.

Pang, Y.-W., and Krovi, V. (2000). "Kinematic Synthesis of Coupled Serial Chain Mechanisms for Planar Path Following Tasks Using Fourier Methods." *ASME 2000 Design and Engineering Technical Conferences and Computers and Information in Engineering Conference*, Baltimore, Maryland.

Rodriguez, N. E. N., Carbone, G., and Ceccarelli, M. (2006). "Optimal design of driving mechanism in a 1-DOF anthropomorphic finger." *Mechanism and Machine Theory*, 41(8), 897-911.

BIOGRAPHICAL SKETCH

Joe Bari was born in Apple Valley, MN. He received B.A. degrees in physics and mathematics at St. Olaf College in Northfield, MN in May, 2008. In August, 2008 Joe joined the Center for Intelligent Machines and Robotics at the University of Florida as a Research assistant. He graduated in December 2009 with a M.S. in mechanical engineering. His research focuses on the design of spatial manipulators.